RSC Advances

ROYAL SOCIETY OF CHEMISTRY

www.rsc.org/advances

RSC Advances

RSCPublishing

ARTICLE

A facile one-step route for production of CuO, NiO, and CuO-NiO nanoparticles and comparison of their catalytic activity for ammonium perchlorate decomposition

Cite this: DOI: 10.1039/xoxxoooooox

Seyed Ghorban Hosseini [a,]* and Reza Abazari [a,b]

Received ooth January 2015,
Accepted ooth January 2015

DOI: 10.1039/xoxxoooooox

www.rsc.org/

This study demonstrates a straightforward, inexpensive, high-yield, and ecofriendly route for synthesis of sphere-like CuO, NiO, and CuO-NiO (with different molar ratios) nanoparticles (NPs) through emulsion route. These NPs have been characterized by scanning electron microscope (SEM), X-ray diffraction (XRD), dynamic light scattering (DLS), and fourier transform infrared spectroscopy (FT-IR). Then, the prepared composites (CuO/AP, NiO/AP, and CuO-NiO/AP) are compared for ammonium perchlorate (AP) decomposition. These composites' thermal decomposition is superior to that of pure AP. Besides, due to their smaller particles size, more active sites, and increased rate of heterogeneous decomposition of deprotonized $HClO_4$ gas on the catalytic surface, CuO-NiO (1:1) NPs show more catalytic activity than CuO and NiO NPs. Here, AP thermal decomposition temperature decreases to around 114.3 ℃. Also, effects of the various CuO/NiO NPs molar ratios on the AP thermal decomposition have been taken into account. Finally, with regard to the AP catalytic thermal decomposition, this study has designed the possible mechanism for the synergistic effect between the suggested NPs.

Introduction

Catalyzed AP thermal decomposition is widely used in aerospace, satellite launching, etc. Since it is the major oxidizer in the composite solid rocket propellants, and rockets ballistics is considerably affected by its burning behavior. As widely known, AP thermal decomposition temperature, reaction rate, and activation energy are tightly linked to the solid propellants characteristics. Therefore, much attention has been paid to the catalytic properties of transition metals and their oxides for AP thermal decomposition.[1-5] Final decomposition temperature is affected by catalytic particle size, type, amount, and its manner of mixture with AP.[5-7] Copper and nickel oxides are quite efficient in AP thermal decomposition, and through their interface, the lifetime of the entrapped excited electrons is prolonged and catalytic activity increases.[2, 3] Moreover, mixed oxides demonstrates more activity than single-component oxides in AP thermal decomposition.[8-12] Accordingly, the synergic mixture of copper and nickel oxides is here suggested to be a desired catalytic system.

It is widely accepted that, as catalysts, the nano-sized particles outperform the bulk or even micro-sized particles. However, nanomaterials can easily be agglomerated because of their small size, large surface area, and high surface activity, which substantially affect their catalytic characteristics. Due to agglomeration, nano-catalytic dispersion is inhomogeneous, catalysts are not in full contact with media, catalytic efficiency decreases, and the costs increase. Besides, the as-synthesized CuO and NiO nanostructures properties are closely related to their size and morphology.[13, 14] Therefore, to address these problems, attempt has already been made to develop novel precursors at ambient conditions. Emulsion method has alternatively been designed for preparing nanostructures with excellent dispersivity, narrow size distribution, controllable morphology, and crystallinity.[15-18] Our proposed method is cost-effective from energy and time standpoints since it can conduct the process in one single step at room temperature.

Here, using CuO-NiO NPs in AP thermal decomposition, a proper catalytic system has been developed. Comparison has been made between the catalytic activity of these NPs and that of its constituent metal oxides (i.e., CuO and NiO NPs). Compared with other samples, CuO-NiO NPs exert an intense catalytic effect on AP decomposition due to the excellent dispersibility, uniform crystallite size, and thorough sphericality of CuO-NiO NPs. Based on our observations, the best catalytic activity of the CuO-NiO nanocomposite was achieved when the molar ratio 1:2 was taken into account. To the best of our knowledge, no report has previously been given on the comparison of catalytic activity of CuO, NiO, and CuO-NiO NPs for the investigation of the catalytic thermal decomposition of AP.

Experimental

Materials

The following chemicals were used in the synthesis procedure: copper(II) sulfate pentahydrate ($CuSO_4.5H_2O$ ≥98%, sigma) and nickel(II) sulfate hexahydrate ($NiSO_4.6H_2O$ 99%, sigma-Aldrich), as precursor salts; dioctyl sulfosuccinate sodium salt (aerosol-OT, AOT 98%, Aldrich) as a surfactant; ammonia solution (NH_4OH 25%) as a reducing agent; isooctane (≥99%, Merck) as the oil phase; methanol (≥99.9%, Merck) as a washing agent and solvent; and water used in the experiments was deionized (DI) and doubly distilled prior to use as the aqueous phase in emulsion system. Also, analytical reagent grade AP powder with mean particle size of 80-100 mm was obtained from Fluka and methyl isobutyl ketone (MIBK, >99%) was purchased from Merck as a non-solvent. Substrates were purchased from Merck Company, and were used without further purification or drying.

RSC Advances RSCPublishing

ARTICLE

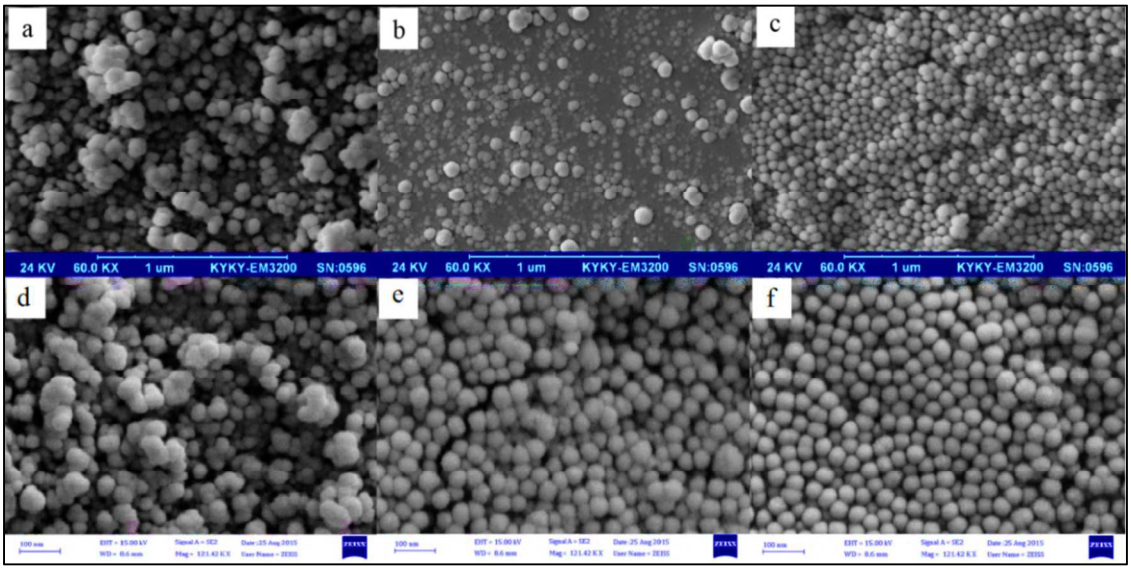

Fig. 1 SEM images of CuO (a), NiO (b), CuO-NiO (1:1) (c), CuO-NiO (2:1) (d), CuO-NiO (1:2) (e), and CuO-NiO (1:3) (f) NPs.

Characterization

The morphology (or shape), crystal structure, and size of the CuO, NiO, and CuO-NiO NPs (with Cu/Ni molar ratios of 1:1, 2:1, 1:2, and 1:3) were characterized by scanning electron microscope (SEM), X–ray diffraction (XRD), dynamic light scattering (DLS), and fourier transform infrared spectroscopy (FT-IR). SEM images were obtained on a KYKY-EM3200 scanning electron microscope using accelerating voltage of 25 kV. To obtain SEM images, the samples were dispersed in ethanol and a drop of this suspension was deposited on a stainless SEM stub. The stub was dried in air at room temperature and coated with gold before characterization. Then, the SEM micrograph was obtained. XRD analysis of these NPs was carried out using a Philips diffractometer (Model TM–1800). Nickel filtered Cu–Kα radiation source was used to produce X–ray (λ = 0.154 nm), and scattered radiation was measured with a proportional counter detector at a scan rate of 4°/min. The scanning angle was from 20° to 80°, operating at a voltage of 40 kV applying potential current of 30 mA. The particle size distribution was measured using Brookhaven 90 Plus, DLS spectrometer. FT–IR spectra (in the wavenumber range from 400 to 4000 cm^{-1}) were recorded using KBr disks on a Shimadzu FT–IR model Prestige 21 spectrometer. Also, TEM measurement for the CuO-NiO (1:2) NPs as the superior catalyst in this work (with Cu/Ni molar ratio of 1/2) was performed on a Philips model EM-208S instrument operated at an accelerating voltage of 100 kV.

Preparation of CuO, NiO, and CuO-NiO NPs by emulsion method

In this study, CuO-NiO NPs with different molar ratios of CuO to NiO (1:1, 2:1, 1:2, and 1:3) were synthesized via emulsion route. CuO-NiO NPs with the molar ratio of 1:1 have been synthesized as follows. The same procedure is also true for the CuO, NiO, and other molar ratios of CuO-NiO NPs. Initially, three emulsions with different aqueous phases containing 0.72 mmol $CuSO_4.5H_2O$, 0. 72 mmol $NiSO_4.6H_2O$ (emulsion A and emulsion B, respectively) and 1.08 mmol NH_4OH (emulsion C) were prepared (note that each emulsion was formed with 1.44 mmol AOT concentration and a given amount of isooctane as the oil phase). Subsequently, emulsion A has been combined with emulsion B so that a homogeneous solution can be obtained. After mechanical agitation for about 30 min, emulsion C was mixed to emulsion A and B. The reaction time was maintained for 2 h with rapid stirring at room temperature in order to CuO-NiO precursor. Then, using ethanol, the particles were washed twice, each of which lasted for10 min. The final mixture was centrifuged to get CuO-NiO precursor and it was dried at 50 ℃. Crystallization of the product was performed by calcination at 400 ℃ for 6 h in air.

Preparation of CuO/AP, NiO/AP, and CuO-NiO/AP composites

CuO-NiO/AP composites were synthesized as follows, while the same procedure is true for the CuO/AP and NiO/AP composites. To evaluate the catalytic activity of the as-prepared CuO-NiO NPs and NH_4ClO_4 (to produce composites) they were thoroughly mixed by the solvent/non-solvent route. This is expected to prevent CuO-NiO species from agglomeration and promote their dispersion resulting in an enhancement of catalytic activity and stability. In this study, water and methyl isobutyl ketone were chosen as the solvent and non-solvent, respectively. First, the CuO-NiO NPs were dispersed in 25 mL methyl isobutyl ketone by ultrasonics. Also, AP was dissolved into the water to make a saturated solution at 65 ℃. The saturated solution of AP was dropwised into the CuO-NiO NPs to obtain a composite of CuO-NiO/AP. In this experiment, AP was mixed with the CuO-NiO NPs at a weight ratio of 97:3. Then, the reaction lasted for several minutes until all the AP was deposited on the surface of the CuO-NiO particles. Finally, the coated particles (i.e., composites) were filtered and washed with 10 mL methyl isobutyl ketone as a non-solvent three times and dried at ambient temperature.

Results and discussion

Optical, electronic, magnetic, and catalytic characteristics of any nanomaterial heavily depend on its size and morphology. Catalytic reactivity and selectivity are also affected by nanomaterial shapes, sizes, and crystallization. Therefore, using SEM analysis, the surface morphology of all synthesized samples was investigated (Fig. 1). Figs. 1a and 1b demonstrate the formation of quasi-spherical aggregates with slight uniform distribution of CuO and NiO NPs, respectively. As indicated by SEM image of CuO-NiO NPs (Fig. 1c, with Cu/Ni molar ratio of 1), the size of CuO-NiO (1:1) NPs is clearly smaller than that of CuO and NiO NPs, which increases the surface area. Moreover, these non-aggregated spherical CuO-NiO (1:1) NPs are highly uniform with the average particle size of 35 nm. This variation in the uniformity of morphology and size might be due to the type and ratio of the precursors, which produces the composite. Also, as shown in Fig. 1d, morphology of the CuO-NiO (2:1) NPs is quite similar to that of the CuO NPs. However, in the case of the CuO-NiO (2:1) NPs, the particle sizes have grown a little larger. Moreover, SEM results analysis of CuO-NiO (1:2) and CuO-NiO (1:3) NPs (Figs. 1e and f) shows that the morphology of the said particles has mostly remained unchanged. However, in this state, the uniformity of the particles is slightly low, compared to the case where the molar ratio of 1:1 (in the CuO-NiO NPs) is applied.

In the next step, XRD, DLS, and FT-IR measurements have been used to characterize the crystallite phases, size, structure, and proof of the formation of prepared NPs (i.e., CuO, NiO, and CuO-NiO NPs with Cu/Ni molar ratios of 1:1. 2:1, 1:2, and 1:3). Using X-Ray diffraction, the nanostructures have been investigated in terms of their solid structure, and the purity of the corresponding phase has also affirmed. The XRD pattern of CuO, NiO, and CuO-NiO NPs is depicted in Fig. 2. XRD pattern of the CuO and NiO NPs by emulsion technique is shown in Fig. 2a and b, respectively. Based on our obtained results, in the vicinity of aerosol-OT, no change occurs in the CuO and NiO structures. The diffraction peaks, both in their peak position and their relative intensity, are observed to be in complete agreement with the standard spectrum (CuO: JCPDS, 89-5899; and NiO: JCPDS, 78e0643). Using Scherer equation and by considering each diffraction peak broadening, the crystallite size of CuO and NiO NPs was obtained to be 58.32 and 43.96 nm, respectively. Also, Fig. 2c shows XRD pattern of CuO-NiO nano-composites with a 1:1 Cu/Ni molar ratio calcinated at 400 ℃ for 6 h. As is clear from XRD pattern, complete conversion of the precursors to CuO-NiO nano-composites has been done. The diffraction peaks for CuO-NiO NPs are indexed to a monoclinic CuO phase (JCPDS card, no. 89-5899) and a cubic NiO phase (JCPDS card, no. 78-0643). This demonstrates the existence of crystalline CuO and NiO in the sample. Besides, no impurity peaks (e.g., $Cu(OH)_2$ or Cu_2O) exist, which shows the phase-pure structure of the CuO-NiO NPs prepared by emulsion method. Average size of CuO-NiO NPs obtained from Debye-Scherrer equation is about 38.65 nm, which is in conformity with SEM results having crystallite size of 40 nm. Moreover, based on the XRD results as shown in Figs. 2d, e, and f no particular change has occurred in the crystalline structure of the CuO-NiO NPs with Cu/Ni molar ratios of 2:1, 1:2, and 1:3, compared to the case where the molar ratio of 1:1 (in the CuO-NiO NPs) is applied. However, by the change of the molar ratio, the intensity and the value of the corresponding peaks might increase or decrease.

Also, particle size distribution was characterized using DLS analysis. In Fig. 3, CuO, NiO, CuO-NiO (1:1), CuO-NiO (2:1), CuO-NiO (1:2), and CuO-NiO (1:3) NPs particle size distribution, based on DLS analysis, is shown, which is in compliance with SEM and PXRD results.

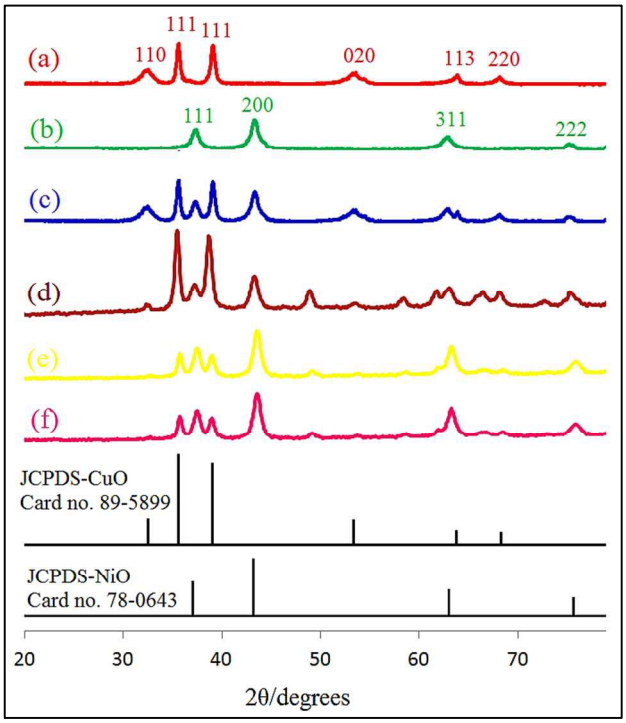

Fig. 2 XRD patterns of the CuO (a), NiO (b), CuO-NiO (1:1) (c), CuO-NiO (2:1) (d), CuO-NiO (1:2) (e), and CuO-NiO (1:3) (f) NPs after calcination at 400 ℃ for 6 h in air.

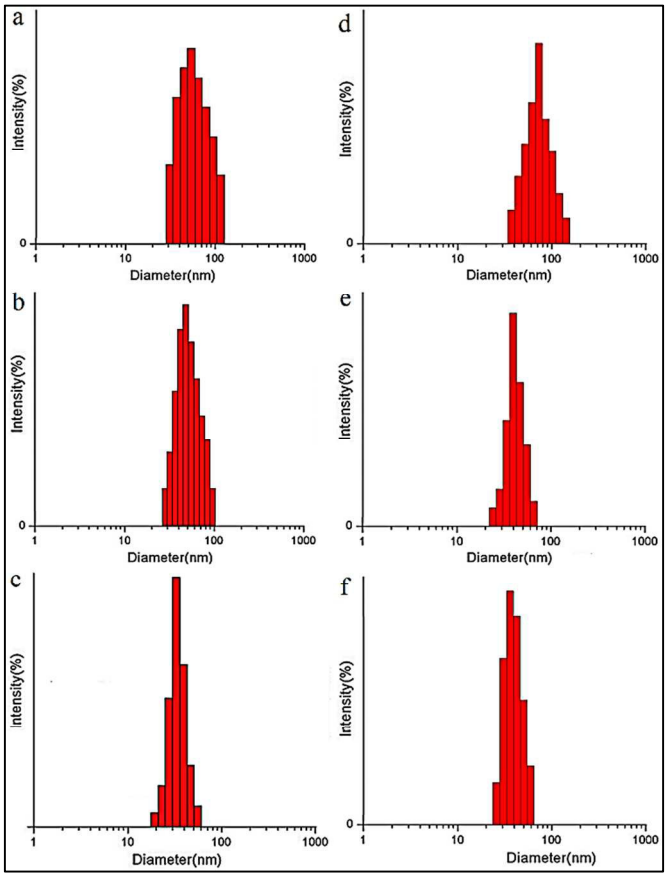

Fig. 3 Particle size distribution of the CuO (a), NiO (b), CuO-NiO (1:1) (c), CuO-NiO (2:1) (d), CuO-NiO (1:2) (e), and CuO-NiO (1:3) (f) NPs produced at the emulsion system.

FT-IR spectroscopy is sensitive to metal–oxygen bonds vibrations, gives crucial information for catalytic structural integrity, and provides an analytical tool for measuring compound purity. For removal of the adsorbed surfactant on NPs surface, CuO, NiO and CuO-NiO NPs calcined at 400 ℃ were evaluated through FT-IR technique. Fig. 4 shows comparative FT-IR spectra of CuO, NiO, CuO-NiO (1:1), CuO-NiO (2:1), CuO-NiO (1:2), and CuO-NiO (1:3) NPs. The peaks at 3438, 1631 and 1381 cm^{-1} are related to the water adsorbed on these NPs surface.[19] The broad band at about 400-500 cm^{-1} of mixed oxides may be due to M-O vibration, which demonstrates the presence of NPs in mixed system.[20] The region lower than 1000 cm^{-1} generally demonstrates the intensive bands in all of the spectra, which are in association with the stretching vibration mod of the M-O bond and thus verify the metal oxide formation.[21, 22] Hence, the broad band at 525 cm^{-1} is attributable to the stretching vibrations of (Cu^{II}-O) while the band at 421.7 cm^{-1} is related to Ni^{II}–O stretching.[17, 23-25] Based on the FT-IR spectrum of CuO-NiO NPs, two remarkable keen-edge peaks are observed in the range of 400–600 cm^{-1}, which can be ascribed to the formation of the CuO-NiO nanocomposite. Also, as indicated by CuO-NiO NPs spectra, no bands are designated corresponding to new spinel formation and during CuO-NiO NPs synthesis, no organic species were considered; therefore, FT-IR spectra agree with XRD pattern.

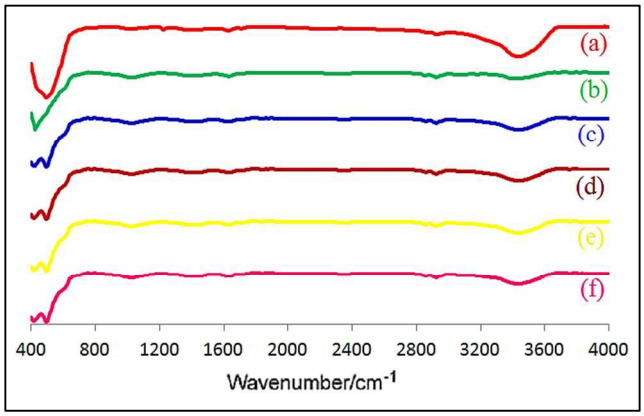

Fig. 4 FT–IR spectras of the CuO (a), NiO (b), CuO-NiO (1:1) (c), CuO-NiO (2:1) (d), CuO-NiO (1:2) (e), and CuO-NiO (1:3) (f) NPs synthesized in water/AOT/isooctane emulsion system.

In the next step and using DSC analysis, the thermal properties and coating quality of the considered samples have been studied. DSC (Fig. 5) curves show AP thermal decomposition influenced by burning rate of CuO, NiO, and CuO-NiO nanoparticles. According to DSC curve for pure AP, during decomposition, three events happen. Fig. 5 shows that the first and the second peaks at 237.8 ℃ and 332.6 ℃ are related to orthorhombic to cubic form transition and partial AP decomposition, respectively. The third exothermic peak about 431.2 ℃ is due to AP thermal decomposition.[1-12] The heat from pure AP equals 769.7 Jg^{-1}.

AP decomposition at high temperatures is both difficult and risky, and hence it is of great importance to prepare appropriate catalysts to reduce AP decomposition temperature. AP catalytic thermal decomposition can be achieved using such metal oxide additives as CuO and NiO catalysts due to their commercial and industrial benefits such as cost-efficiency, excellent catalytic activity, non-toxicity, and high chemical stability. Besides, nano-sized composite materials outperform the non-composites since their electronic, magnetic, catalytic, optical, and thermal characteristics are improved.[8, 26] Although individual properties of CuO or NiO are widely recognized, scant attention has already been paid to the catalytic CuO-NiO composite nanostructures for AP thermal decomposition. Thus, the present paper has considered the catalytic application of the mixed metal oxide of CuO-NiO for AP decomposition. As demonstrated by DSC data, marked differences are observed in AP decomposition patterns of CuO, NiO, and CuO-NiO (1:1) NPs. The endothermic peaks at about 235–238 ℃ in all samples initially showed a similar shape, and hence AP crystallographic transition temperature was not much affected by additives. However, the exothermic peaks of AP decomposition drastically changed. Addition of CuO, NiO, and CuO-NiO (1:1) NPs resulted in the appearance of sharper exothermic peaks at a lower temperature. More accurately, in the presence of CuO and NiO nano-catalysts, a significant decrease occurred in the first and second decomposition temperature of AP. However, the use of CuO-NiO NPs facilitated the CuO-NiO/AP composite decomposition process, and original exothermic peak of pure AP at 431.2 ℃ disappeared and merged into one exothermic peak. The original exothermic peak temperature was 345.6, 366.1, and 316.9 ℃ for CuO, NiO, and CuO-NiO (1:1) NPs, respectively. Due to their mixed valence of Cu^{2+} and Ni^{2+} and their unique morphology, CuO-NiO (1:1) nano-composites demonstrate a higher catalytic capacity than most other reported materials. Also, with the decreased catalytic size, the surface area and catalytic activity (as mainly a surface phenomenon) increase. As shown by FE-SEM images, CuO-NiO (1:1) NPs are more spherical and uniform than CuO and NiO NPs. We suggest that due to these similar morphologies, mass transport of AP molecules on all CuO-NiO NPs surfaces is performed with a fixed ratio and more homogeneity. In other words, with more homogeneous NPs, surface-to-volume ratio of the particles uniformly increases and access to mass transport of AP molecules over catalytic surface becomes similar.

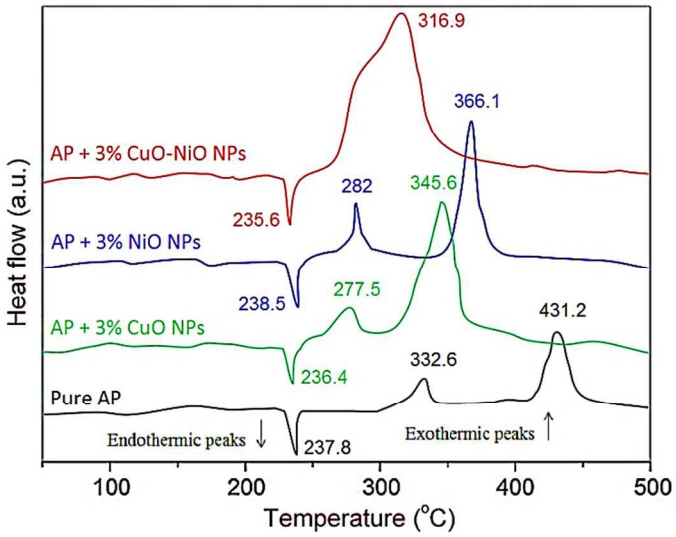

Fig. 5 DSC curves for pure AP and for AP mixed with additives of CuO, NiO, and CuO-NiO (1:1) NPs.

Using CuO-NiO (1:1) catalyst, the high heat released (ΔH) of 1596.5 Jg^{-1} was achieved, which is about 2.07 times that of the pure AP (769.7 Jg^{-1}). From DSC results, the apparent heat released of AP added to CuO, NiO, and CuO-NiO (1:1) NPs samples are 1321.4, 1185.7, and 1596.5 Jg^{-1}, respectively, which – quite similar to their ascending trend of catalytic efficiency – considerably increased by 551.7, 416, and 826.8 Jg^{-1} compared to pure AP. Accordingly, adding CuO-NiO NPs (with Cu/Ni molar ratio of 1), further decrease in AP decomposition temperature and more increase in weight loss rate and decomposition reaction heat were observed. Also, the

unique morphology and smaller size of CuO-NiO (1:1) NPs are appropriate for perchloric acid adsorption and diffusion through Lewis acid-base interactions. Resultantly, AP activation energy decreases and formation of superoxide radical anions and holes is facilitated, which paves the way for more complete oxidation reaction of ammonia in the AP catalytic decomposition.

Since the CuO-NiO (1:1) NPs show more catalytic activity than their constituent oxides (i.e., CuO and NiO), in the next stage, the different molar ratios between these two metal oxides in the CuO-NiO NPs for the AP thermal decomposition have been taken into account. In this context, in order to determine the optimal molar ratio between CuO and NiO in CuO-NiO NPs, first the molar ratios of 2:1 and 1:2 between the aforesaid oxides the AP thermal decomposition were examined. Through the consideration of the molar ratio of 2:1 between CuO and NiO particles, the catalytic activity slightly decreased. As shown in Fig. 6, although the transformation of the two exothermic peaks into one exothermic peak still occurs, nevertheless a slight decrease in the decomposition temperature for the main peak can be seen. As the results show, the decomposition temperature has risen from 316.9 to 354.2 ℃, whereas the decomposition heat has decreased from 1596.5 to 1532.7 Jg^{-1}. If the molar ratio of 1:2 is considered between CuO and NiO, then satisfactory results are obtained. As Fig. 6 shows, the decomposition temperature drops to 309.1 ℃ while the decomposition heat is equal to 1597.3 Jg^{-1}. Since this molar ratio provides better results than the molar ratio of 1:1 between the said oxides, in the next stage, the molar ratio of 1:3 was also taken into account so that the results might be further improved. However, under this scenario, the catalytic activity of CuO-NiO (1:3) NPs decreased, and consequently the decomposition temperature and decomposition heat were obtained to be 328.6 ℃ and 1561.4 Jg^{-1}, respectively. Therefore, it can be suggested that the best molar ratio between these two metal oxides in the CuO-NiO/AP composite with respect to the considered catalytic system is 1:2.

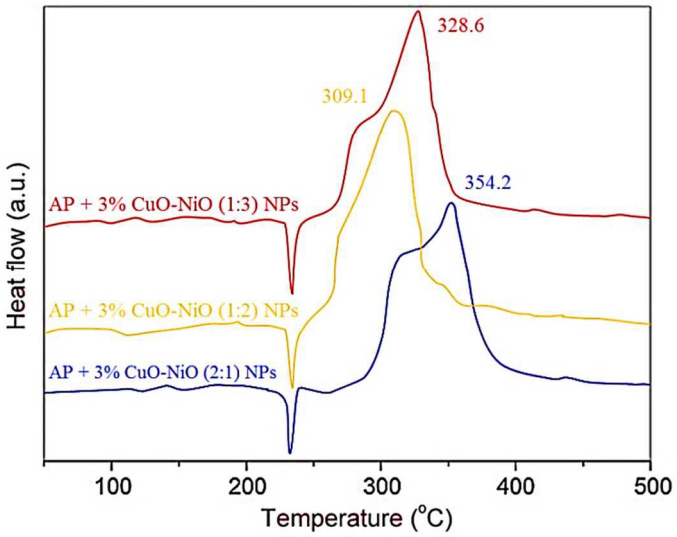

Fig. 6 DSC curves for AP mixed with additives of CuO-NiO (2:1), CuO-NiO (1:2), and CuO-NiO (1:3) NPs.

In order to determine the different catalytic characteristics of the CuO-NiO NPs with the molar ratio of 1:2 and to investigate the probable effects of variations in the morphology, and structure on the catalytic activity of the CuO-NiO (1:2) NPs, the said NPs have thus been characterized using TEM analysis. Using the TEM analysis for the more exact study of the morphology of the CuO-NiO NPs with the molar ratio of 1:2 (as the superior catalyst in our work), the results were found to be in better compliance with the results of the SEM analysis (Fig. 7). Besides, the particles were observed to keep their sphericality with respect to the change in the molar ratio. Therefore, another reason must be found for the better catalytic activity of the CuO-NiO NPs with the molar ratio of 1:2 than that of the said nanocomposite with the molar ratio of 1:1. Since the catalytic activity of the suggested NPs with the molar ratio of 1:2 is better than that of the said NPs with the molar ratio of 1:1, it can be suggested that the NiO plays a more important role in the catalytic procedure cycle. As an example, some members of our research group have already discussed in detail the great importance of the molar ratio of the catalyst Pt/Pd/Fe in the catalytic cycle in the hydrodehalogenation reaction. Based on our previous findings, as the molar ratio of a given element in a compound increases, its related importance in the catalytic system is likely to increase.[27]

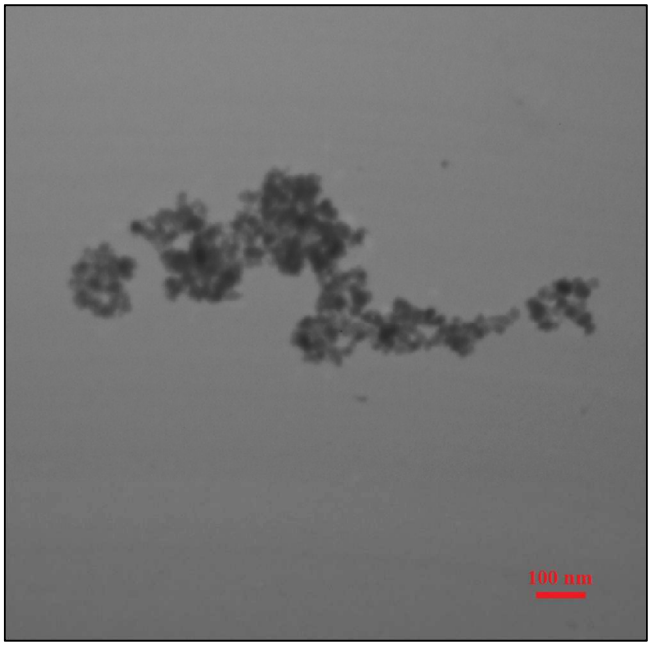

Fig. 7 TEM image of spherical CuO-NiO (1:2) NPs formed in the emulsion nanoreactors, scale bar is 100 nm.

Therefore, the CuO-NiO NPs outperforms either of its constituent parts (i.e., CuO or NiO) in terms of their related catalytic activities, which seems to be due to the synergistic relation between CuO and NiO in the CuO-NiO NPs. In this regard, through the consideration of the electron transfer processes, a mechanism for the decomposition of the AP in the presence of CuO-NiO NPs has been proposed. A brief review of the recent literature shows that,[28-30] the AP thermal decomposition can be conducted within a proper framework. To this end, electrons are first to be transferred from the perchlorate ion to the ammonium ion. This procedure can be expressed as follows.

$$ClO_4^- + NH_4^+ \rightarrow ClO_4^0 + NH_4^0$$
$$NH_4^0 \rightarrow NH_3 + H$$
$$ClO_4^0 + ClO_4^- = ClO_4^- + ClO_4^0$$
$$HClO_4 + H \rightarrow H_2O + ClO_3$$

Based on the said mechanism, as the electrons are transferred from anion to cation, the decomposition process takes place.

$$ClO_4^- + NH_4^+ \rightarrow ClO_4^0 + NH_4^0$$

As the probability of the electron realization increases, the ions become less distanced from each other. Therefore, in place of the ammonium ion, the ions located in interstices are to be used as effective acceptors of electrons. After electrons are accepted, decomposition of the ammonium radicals into ammonia and hydrogen atom occurs.

$$NH_4^0 \rightarrow NH_3 + H$$

In this context, atomic hydrogen moves over the lattice. Exactly in the same way, electrons migrate over the anion sublattice:

$$ClO_4^0 + ClO_4^- = ClO_4^- + ClO_4^0$$

$HClO_4$ is produced due to the interaction between ClO_4 radical and H. The resultant $HClO_4$ might also continue to interact with H, thus:

$$HClO_4 + H \rightarrow H_2O + ClO_3$$

Indeed, electrons are trapped by the ClO_3 radical. When electrons are trapped, they are then transformed into ClO_3^- ion. Subsequently, chlorite ion and ClO_4 radical are decomposed. Then, the decomposed products interact with NH_4^+ ions. Due to this interaction, secondary products such as chlorine, nitrogen hemi oxide, and water are formed.
Then, it is required to transfer protons from the ammonium ion to the perchlorate ion. The related process can be written as follows.

$$NH_4ClO_{4(s)} \rightarrow ClO_4^- + NH_4^+ \rightarrow NH_{3(s)} + HClO_{4(s)} \rightarrow NH_{3(g)} + HClO_{4(g)}$$

Under this scenario, the electron transfer stage is presumed to be the rate control one.[31] Furthermore, due to the p-type semi-conductivity of both CuO and NiO oxides as well as their related nanocomposite (i.e., CuO-NiO) and with regard to the existence of some positive holes on the catalytic surface of the said catalytic particles for reception of the electrons released from the perchlorate ion, they are assumed to speed up the process of transferring electrons.

$$e^-_{oxide} + ClO_4^- \rightarrow O_{oxide} + ClO_3^- \rightarrow \frac{1}{2}O_2 + ClO_3^- + e^-_{oxide}$$

Here, the effective positive site in the oxide's valance band is signified by e^-_{oxide}. Besides, O_{oxide} shows a separated atom of oxygen from the aforementioned oxide. As is widely recognized, the mechanism can be divided into two substantial sub-procedures as oxidation of the ammonia and ClO_4^- species dissolving into ClO_3^- and O_2. In order to oxidize ammonia, high and stable catalytic activities are demonstrated by the metal oxides. On the other hand, as the process goes on, the released electrons from the oxidation of ammonia are accepted by the metal oxides. This in turn helps in further dissociation of ClO_4^- species into ClO_3^- and O_2.[31]

As it has already been discussed, the CuO-NiO NPs outperforms either of its constituent parts (i.e., CuO or NiO) with respect to its catalytic behavior towards the AP thermal decomposition. The catalytic superiority of the said NPs over its constituent oxides can be explained by the fact that the 3d orbital of CuO-NiO structure is relatively filled. In other words, in the considered NPs structure, a partially filled 3d-orbital always exists for Cu^{2+} and Ni^{2+}. Compared to the single metal oxides, in CuO-NiO NPs, both metal oxides can simultaneously participate in the electron transfer procedure. In our suggested mechanism, first the existing Ni^{2+} in the catalytic system accepts the released electron from ClO_4^-, and thus ClO_4^- is changed into CLO_4. In the next stage, the provided unstable form of Ni^{1+} easily participates in another electron transfer procedure, and consequently it causes the Cu^{2+} ($3d^9$) to be changed into the stable full-filled 3d-orbital form of Cu^+ ($3d^{10}$). On the other hand, as recorded in the literature, synergistic effects are likely to happen between these two metal oxides, which in turn results in the creation of the active sites of Cu^+ and Ni^{3+} that help in conduction of the catalytic process and chemisorption .[32] Therefore, the prepared Ni^{3+} in this process can also participate in another electron transfer procedure and paves the way for the creation of CLO_4 species from ClO_4^- through the process of electron acceptance, while the said Ni^{3+} finally changes into the more stable form of Ni^{2+}. In this regard, the above explanation can be considered as a possible reason behind the catalytic performance superiority of the CuO-NiO nanocomposite over its constituting oxides. In other words, CuO-NiO nanoparticles produce a positive synergistic catalytic effect.

$$Ni^{+2} + ClO_4^- \rightarrow Ni^{+1} + ClO_4$$
$$Ni^{+1} + Cu^{+2} \rightarrow Ni^{+2} + Cu^{+1}$$
$$Ni^{+2} + Cu^{+2} \rightarrow Ni^{+3} + Cu^{+1}$$
$$Ni^{+3} + ClO_4^- \rightarrow Ni^{+2} + ClO_4$$

Furthermore, the optimal molar ratio in the present study is in total agreement with the proposed mechanism, which is due to the prominent role of nickel in directly setting the ground of changing ClO_4^- into ClO_4 for two times. However, when the molar ratio rises to 1:3 (CuO-NiO), the role of Cu^{2+} seems to diminish, and hence the transformation of Ni^{1+} into Ni^{2+} becomes difficult.

On the other hand, the catalytic superiority of our considered nanocomposite can also be explained in terms of the charge transfer effect between the metal oxides of the said NPs, which possibly reduces the AP thermal decomposition activation energy. In the present study, it has also been suggested that the positive holes and electrons on the catalytic surface are probably created by the so-called Cu^{2+} John–Teller effect or the lattice defects in the CuO-NiO NPs. Consequently, CuO-NiO (1:2) NPs are suggested as a promising material for AP-based propellants.

Conclusion

This study has prepared quite spherical CuO, NiO, and CuO-NiO NPs in ambient conditions in the absence of any co-surfactant. Using DSC measurements, the catalytic effect of these as-synthesized samples on AP thermal decomposition has been studied. Based on the results, using such NPs, the reaction rate considerably increases while activation energy decreases. Adding 3% of CuO-NiO (1:1) NPs to AP, the decomposition temperature drops by 114.3 ℃ while decomposition heat increases from 769.7 to 1596.5 Jg^{-1}. Also, through the investigation of different molar ratios of CuO-NiO NPs for the thermal decomposition of AP, it has been found that the best molar ratio between these two metal oxides is equal to 1:2. This superior catalyst was further characterized using the TEM analysis. Based on our proposed mechanism, the said situation seems to be due to the existence of a synergistic relation between CuO and NiO particles. The substantial decrease in activation energy shows the higher catalytic efficiency of these NPs, which is due to their shift from bulk-to-nanostructure, reduced size, pure phase, and more uniformity and sphericality. Therefore, our prepared composites seem to be particularly promising for further applications in terms of the composite solid rocket propellants.

Notes and references

[a] Department of Chemistry, Malek Ashtar University of Technology, P.O. Box 16765-3454, Tehran, Iran
Corresponding author: hoseinitol@yahoo.com (S. G. Hosseini);

Tel/fax: (+9821) 22943678.
r.abazari@sina.kntu.ac.ir (R. Abazari).
[b] Department of Chemistry, Tarbiat Modares University, P.O. Box 14115-175, Tehran, Iran

1 Q. Li, Y. He and R. Peng, Graphitic carbon nitride (g-C_3N_4) as a metal-free catalyst for thermal decomposition of ammonium perchlorate, *RSC Adv*., 2015, **5**, 24507–24512.
2 Y. Wang, J. Zhu, X. Yang, L. Lu and X. Wang, Preparation of NiO nanoparticles and their catalytic activity in the thermal decomposition of ammonium perchlorate, *Thermochim. Acta*, 2005, **437**, 106–109.
3 C. Yang, F. Xiao, J. Wang and X. Su, Synthesis and microwave modification of CuO nanoparticles: Crystallinity and morphological variations, catalysis, and gas sensing, *J. Colloid Interface Sci*., 2014, **435**, 34–42.
4 J.-M. Yang, W. Zhang, Q. Liua and W.-Y. Sun, Porous ZnO and ZnO-NiO composite nano/microspheres: synthesis, catalytic and biosensor properties, *RSC Adv*., 2014, **4**, 51098–51104.
5 S. G. Hosseini, R. Abazari and A. Gavi, Pure $CuCr_2O_4$ nanoparticles: Synthesis, characterization and their morphological and size effects on the catalytic thermal decomposition of ammonium perchlorate, *Solid State Sci*., 2014, **37**, 72–79.
6 B. A. McDonald, J. R. Rice and M. W. Kirkham, Humidity induced burning rate degradation of an iron oxide catalyzed ammonium perchlorate/HTPB composite propellant, *Combust. Flame*, 2014, **161**, 363–369.
7 H. Zhao, L. Guo, S. Chen and Z. Bian, Synthesis, complexation of 1,2,3-(NH)-triazolylferrocene derivatives and their catalytic effect on thermal decomposition of ammonium perchlorate, *RSC Adv*., 2013, **3**, 19929–19932.
8 H. Liu, Q. Jiao, Y. Zhao, H. Li, C. Sun, X. Li and H. Wu, Cu/Fe hydrotalcite derived mixed oxides as new catalyst for thermal decomposition of ammonium perchlorate, *Mater. Lett*., 2010, **64**, 1698–1700.
9 Z. Li, X. Xiang, L. Bai and F. Li, A nanocomposite precursor strategy to mixed-metal oxides with excellent catalytic activity for thermal decomposition of ammonium perchlorate, *Appl. Clay Sci*., 2012, **65–66**, 14–20.
10 X. Zheng, P. Li, S. Zheng and Y. Zhang, Thermal decomposition of ammonium perchlorate in the presence of $Cu(OH)_2{\cdot}2Cr(OH)_3$ nanoparticles, *Powder Technol*., 2014, **268**, 446–451.
11 X.-F. Guan, J. Zheng, M.-L. Zhao, L. P. Li and G.-S. Li, Synthesis of $FeTiO_3$ nanosheets with {0001} facets exposed: enhanced electrochemical performance and catalytic activity, *RSC Adv*., 2013, **3**, 13635–13641.
12 X. Guan, L. Li, J. Zheng and G. Li, $MgAl_2O_4$ nanoparticles: A new low-density additive for accelerating thermal decomposition of ammonium perchlorate, *RSC Adv*., 2011, **1**, 1808–1814.
13 M. Farboda, R. Kouhpeymani asl and A. R. Noghreh abadi, Morphology dependence of thermal and rheological properties of oil-based nanofluids of CuO nanostructures, *Colloids Surf., A*, 2015, **474**, 71–75.
14 K. Anandan and V. Rajendran, Morphological and size effects of NiO nanoparticles via solvothermal process and their optical properties, *Mater. Sci. Semicond. Process*., 2011, **14**, 43–47.
15 F. Heshmatpour and R. Abazari, Formation of dispersed palladium–nickel bimetallic nanoparticles in microemulsions: synthesis, characterization, and their use as efficient heterogeneous recyclable catalysts for the amination reactions of aryl chlorides under mild conditions, *RSC Adv*., 2014, **4**, 55815–55826.
16 R. Abazari, A. R. Mahjoub and S. Sanati, A facile and efficient preparation of anatase titania nanoparticles in micelle nanoreactors: morphology, structure, and their high photocatalytic activity under UV light illumination, *RSC Adv*., 2014, **4**, 56406–56414.
17 F. Fazlali, A. R Mahjoub and R. Abazari, A new route for synthesis of spherical NiO nanoparticles via emulsion nano-reactors with Enhanced Photocatalytic Activity, *Solid State Sci*., 2015, **48**, 263–269.
18 R. Abazari and S. Sanati, Room temperature synthesis of tungsten (VI) tri-oxide nanoparticles with one-pot multi-component reaction in emulsion nanoreactors stabilized by aerosol-OT, *Mater. Lett*., 2013, **173**, 329–332.
19 R. Abazari, A. R. Mahjoub, L. A. Saghatforoush and S. Sanati, Characterization and optical properties of spherical WO_3 nanoparticles synthesized via the reverse microemulsion process and their photocatalytic behavior, *Mater. Lett*., 2014, **133**, 208–211.
20 R. Abazari, S. Sanati and L. A. Saghatforoush, A unique and facile preparation of lanthanum ferrite nanoparticles in emulsion nanoreactors: Morphology, structure, and efficient photocatalysis, *Mater. Sci. Semicond. Process*., 2014, **25**, 301–306.
21 M. Salavati-Niasari, N. Mir and F. Davar, Synthesis and characterization of Co_3O_4 nanorods by thermal decomposition of cobalt oxalate, *J. Phys. Chem. Solids*, 2009, **70**, 847–852.
22 M. A. Gabal, A. A. El-Bellihi and S. S. Ata-Allah, Effect of calcination temperature on Co(II) oxalate dehydrate-iron(II) oxalate dihydrate mixture: DTA–TG, XRD, Mössbauer, FT-IR and SEM studies, *Mater. Chem. Phys*., 2003, **81**, 84–92.
23 L. Chen, L. Li and G. Li, Synthesis of CuO nanorods and their catalytic activity in the thermal decomposition of ammonium perchlorate, *J. Alloys Compd*., 2008, **464**, 532–536.
24 N. Bayal and P. Jeevanandam, Synthesis of CuO@NiO core-shell nanoparticles by homogeneous precipitation method, *J. Alloys Compd*., 2012, **537**, 232–241.
25 N. Dharmaraj, P. Prabu, S. Nagarajan, C. H. Kim, J. H. Park and H. Y. Kim, Synthesis of nickel oxide nanoparticles using nickel acetate and poly(vinyl acetate) precursor, *Mater. Sci. Eng., B*, 2006, **128**, 111–114.
26 N. G. Cho, H.-S. Woo, J.-H. Lee and I.-D. Kim, Thin-walled NiO tubes functionalized with catalytic Pt for highly selective C_2H_5OH sensors using electrospun fibers as a sacrificial template, *Chem. Commun*., 2011, **47**, 11300–11302.
27 R. Abazari, F. Heshmatpour, and S. Balalaie, Pt/Pd/Fe trimetallic nanoparticle produced via reverse micelle technique: synthesis, characterization, and its use as an efficient catalyst for reductive hydrodehalogenation of aryl and aliphatic halides under mild conditions, *ACS Catal*., 2013, **3**, 139−149.
28 R. Zhu and M. C. Lin, Mechanism and Kinetics for Ammonium Perchlorate Sublimation: A First-principles Study, *J. Phys. Chem. C*, 2008, 112, 14481–14485.
29 E. Alizadeh-Gheshlaghi, B. Shaabani, A. Khodayari, Y. Azizian-Kalandaragh and R, Rahimi, Investigation of the catalytic activity of nano-sized CuO, Co_3O_4 and $CuCo_2O_4$ powders on thermal decomposition of ammonium perchlorate, *Powder Technol*., 2012, **217**, 330–339.
30 P. W. M. Jacobs and H. M. Whitehead, Decomposition and combustion of ammonium perchlorate, *Chem. Rev*., 1969, **69**, 551–590.
31 S. Chaturvedi and P. N. Dave, Nano-metal oxide: potential catalyst on thermal decomposition of ammonium perchlorate, *J. Exp. Nanosci*., 2011, **7**, 205–231.
32 G. A. El-Shobaky, N. R. E. Radwan, M. S. El-Shall, A. M. Turky and H. M.A. Hassan, The role of method of preparation of CuO–NiO system on its physicochemical surface and catalytic properties, *Colloids Surf., A*, 2007, **311**, 161–169.

Graphical Abstract